A proposal to determine the distribution of lateral forces from loaded recycled plastic drainage kerbs

O'FLAHERTY, Fin <http://orcid.org/0000-0003-3121-0492> and AL-SHAWI, Fathi

Research Article

A proposal to determine the distribution of lateral forces from loaded recycled plastic drainage kerbs

Fin O'Flaherty[1] · Fathi Al-Shawi[1]

Received: 14 May 2020 / Accepted: 21 December 2020

Abstract
This study presents a detailed analysis of the lateral forces generated as a result of vertically applied loads to recycled plastic drainage kerbs. These kerbs are a relatively new addition to road infrastructure projects. When concrete is used to form road drainage kerbs, its deformation is minimum when stressed under heavy axle loads. Although recycled plastic kerbs are more environmentally friendly as a construction product, they are less stiff than concrete and tend to deform more under loading leading to a bursting type, lateral force being applied to the haunch materials, the magnitude of which is unknown. A method is proposed for establishing the distribution of these lateral forces resulting from deformation under laboratory test conditions. A load of 400 kN is applied onto a total of six typical kerbs in the laboratory in accordance with the test standard. The drainage kerbs are surrounded with 150 mm of concrete to the front and rear haunch and underneath as is normal during installation. The lateral forces exerted on the concrete surround as a result of deformation of the plastic kerbs are determined via a strain measuring device. Analysis of the test data allows the magnitude of the lateral forces to the surrounding media to be determined and, thereby, ensuring the haunch materials are not over-stressed as a result. The proposed test methodology and subsequent analysis allows for an important laboratory-based assessment of any typical recycled plastic drainage kerbs to be conducted to ensure they are fit-for-purpose in the field.

Keywords Recycled plastic drainage kerbs · D400 load · Pavement · Haunch · Asphalt

1 Introduction

Combined kerb and drainage systems form an integral part of many infrastructure projects with the dual purpose of water removal and delineation, for example providing the circumference of a roundabout or edging for a footpath. Their location very much influences the level of impact they are subjected to, for example, they can be used for highly trafficked applications such as major and minor highways or lower traffic densities such as car parks and landscaping. Applications near industrial parks are particularly vulnerable since heavy goods vehicles operate in the vicinity and impact forces can be much greater. There are different types of drainage kerbs on the market, the majority being concrete based but with additives included to enhance performance. Others are made from recycled plastic which are lighter than concrete, therefore, mitigate the risks associated with heavy lifting to the construction workers [1].

It is well known that plastic contamination has become a major issue in recent years hence there has been a drive to reuse this waste material in different ways. For example, there has been a surge in research in recent years into the use of waste plastic as a constituent in construction-related materials. In addition to recycled plastic drainage kerbs, development of paving blocks has received

✉ Fin O'Flaherty, f.j.oflaherty@shu.ac.uk; Fathi Al-Shawi, f.al-shawi@shu.ac.uk | [1]Centre for Infrastructure Management, Materials and Engineering Research Institute, Sheffield Hallam University, Howard Street, Sheffield S1 1WB, UK.

Published online: 22 January 2021

considerable attention [2–6] as have other concrete based materials [7–10]. Waste plastic has also been used as a replacement for cement [11], coarse [12, 13] and fine [14, 15] aggregates in concrete and for developing a plastic type binder in mortar [16]. Bricks containing waste plastic have also been developed [17, 18]. However, the quantity of waste plastic used in these developments will vary as the plastic is added primarily as a constituent. The recycled plastic drainage kerb has a high waste plastic content, therefore, will help alleviate the waste plastic problem that currently exists. Further information on the recycled plastic drainage kerbs is given in Sect. 3.

Although they are designed to provide the same water management solution as concrete kerbs, their method of installation differs in that they need protection in the form of a U-shaped cradle-like concrete surround to the front and rear haunch and bed under the kerbs[1]. In instances where fast moving traffic is present, kerbs are required to be able to withstand vertically applied test loads of 400 kN under laboratory conditions (Class D400 [19]). Further support is then provided via the road construction at the front of the kerb or landscaped area/footpath if present behind the rear haunch.

Since recycled plastic kerbs are less-stiffer than concrete, they tend to deform more under loading leading to a bursting type, lateral force being applied to the haunch materials. The purpose of this paper is to develop a proposal for predicting the influence of the lateral forces on the haunch materials as a result of deformation under load. A load of 400 kN, as required by the test standard [19] was applied onto six recycled plastic drainage kerbs across two sizes in the laboratory and the lateral forces exerted as a result of deformation was measured on a strain measuring system. This load also aligns with Load model 2 (Clause 4.33 + National Annex 2.15) from the relevant bridge design standard (BS EN 1991 [20]). The laboratory results are related to the tensile strength of the concrete surround and pavement design characteristics as given in the Design Manual for Road and Bridges, DMRB 26/06 [21] regarding the depth of road construction materials (e.g. depth of asphalt road surface). Although the loading tests were conducted on recycled plastic drainage kerbs from one manufacturer, the main aim was to develop and prove the concept for testing any type of recycled plastic drainage kerbs. The results can be used to ensure that haunch materials with suitable strength properties are specified to ensure the drainage kerbs are properly restrained on site.

Following the Introduction given in this section, the significance of the research is presented in Sect. 2. Information on the selection of the specimens and their preparation for testing is given in Sect. 3. The loading arrangement for the test specimen is given in Sect. 4 followed by the test results in Sect. 5. Detailed analysis of the test data is given in Sect. 6 and includes an estimation of the lateral bursting forces and resulting stress in the concrete surround. A discussion of the results is given in Sect. 7 followed by the main conclusions from the research in Sect. 8. The paper is completed with acknowledgements, conflict of interest statement and references.

2 Research significance

In comparison with concrete, recycled drainage plastic kerbs are a relatively new addition to road infrastructure projects. It is well known that concrete is a stiff material and when used to form road drainage kerbs, its deformation is minimum when stressed under heavy axle loads. However, when loaded horizontally as in the case of wheel impact, the concrete drainage kerb may suffer impact damage if the force is large enough or displacement depending on its level of embedded support. However, in terms of testing all kerbs to ensure they meet the specification for strength [19], a vertical load only of 400 kN is applied perpendicular to the surface of the test unit and through the geometric centre of the test unit (horizontal loads are not applied). The load is uniformly distributed over the whole surface of the test specimen.

However, recycled plastic is not as stiff as concrete, and although it can offer better impact resistance and is lighter for handling purposes, the kerbs can be prone to more deformation compared to concrete drainage kerbs under load. This means that the plastic drainage kerbs will have a tendency to exert force in the lateral direction due to deformation. The magnitude of this lateral force is unknown meaning it is not clear how much force is exerted into the haunch materials in front or behind the drainage kerbs. The research presented in this paper is novel in that no other information exists on the magnitude of these typical bursting forces. An indication of the resulting stress transferred to the concrete surround and into the haunch materials is required so the system can be properly designed to ensure complete confinement of the recycled plastic drainage kerb based on standardised laboratory testing.

[1] Sometimes concrete is provided underneath and to the rear haunch only and the road construction to the front provides the restraint

Fig. 1 Moulds for six kerbs at the casting stage

3 Specimen selection and preparation

The main constituents in the recycled drainage plastic kerbs are recycled plastic and special binders to give the composite the required strength. However, the precise constituents can vary from manufacturer to manufacturer and it is their responsibility that their kerbs are fit-for-purpose for on-site use (information on the precise constituents is commercially sensitive information). Each manufacturer must be ISO accredited (9001) and products must carry third party accreditation. The kerbs must also comply with Highways Agency specification Appendix 5/5 Clause 516 (Combined Drainage Systems) in the UK [22].

Two different sized recycled plastic drainage kerbs were randomly selected for testing. The drainage kerbs were either 305 or 480 mm deep so for simplicity, will be referred to '305' or '480'. Kerbs with a splay profile were chosen for testing as opposed to the half battered. Three samples were tested per kerb depth. Test results were averaged as shown in Sect. 5.

Plywood moulds were used to support the drainage kerb and concrete during casting (Fig. 1). The drainage kerbs were accurately located within the mould to ensure the 150 mm thickness of concrete was consistent on the front and rear haunch and underneath. The aim was to have a concrete with a 28 days strength greater than 20 MPa (ST4 mix), but due to time limitations, a high strength mix was specified so testing could be done after 7 days. The rear haunch was filled with concrete to the appropriate height (underside of lip, 50 mm from the top of the kerb) whereas the concrete at the front of the kerb was filled to the drainage inlets (Fig. 2). The specimens were de-moulded after five days and left to cure externally for a further two days (covered with polyethlene sheets). Concrete cubes measuring 100 × 100 × 100 mm were cast

Fig. 2 Demoulded kerb

simultaneously to determine the concrete strength at the time of load application to the drainage kerbs (approx. 23 MPa). Testing was done in accordance with BS EN 1881 [23] (which has since been superseded by BS EN 12390 [24]).

4 Loading arrangement

The drainage kerbs were manually located onto the bed of a test frame and the load was applied (rate: 2 ± 1 kN/s) via a hydraulic jack, electric pump and steel loading beams in accordance with [19] (used to apply the load uniformly onto the top of the kerb, Fig. 3a, b. The loading beam was shaped to match the contact face of the test block. The capacity of the cylinder was 50 Te (25% greater than the test load class D400 as required by the test standard [19]). The load was monitored via a calibrated load cell in metric tonnes which was converted to kN.

In order to measure the lateral forces exerted (a measurement that is not required under the existing standard but was included here for research purposes [19]), a strain measuring system consisting of 6 mm diameter high tensile steel threaded tie rods and four steel channel Sects. (150 × 76 mm) were used as shown in Fig. 3. The steel rods were instrumented with vibrating wire strain gauges, the strains would ultimately be used to determine the bursting (lateral) forces. The threaded bars were supplied

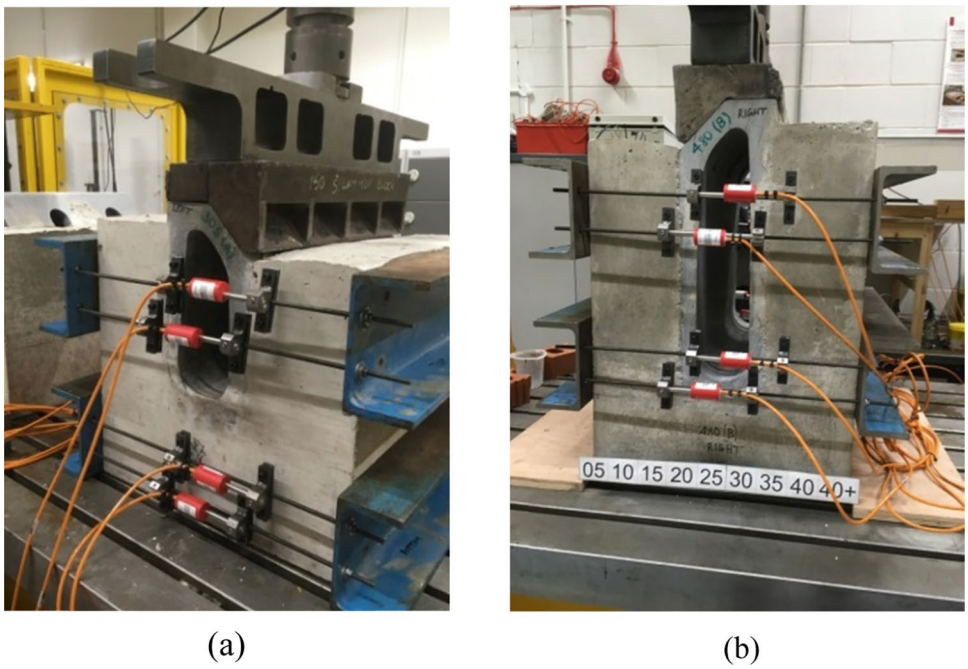

Fig. 3 Recycled plastic drainage kerbs at set-up: **a** 305 mm; **b** 480 mm

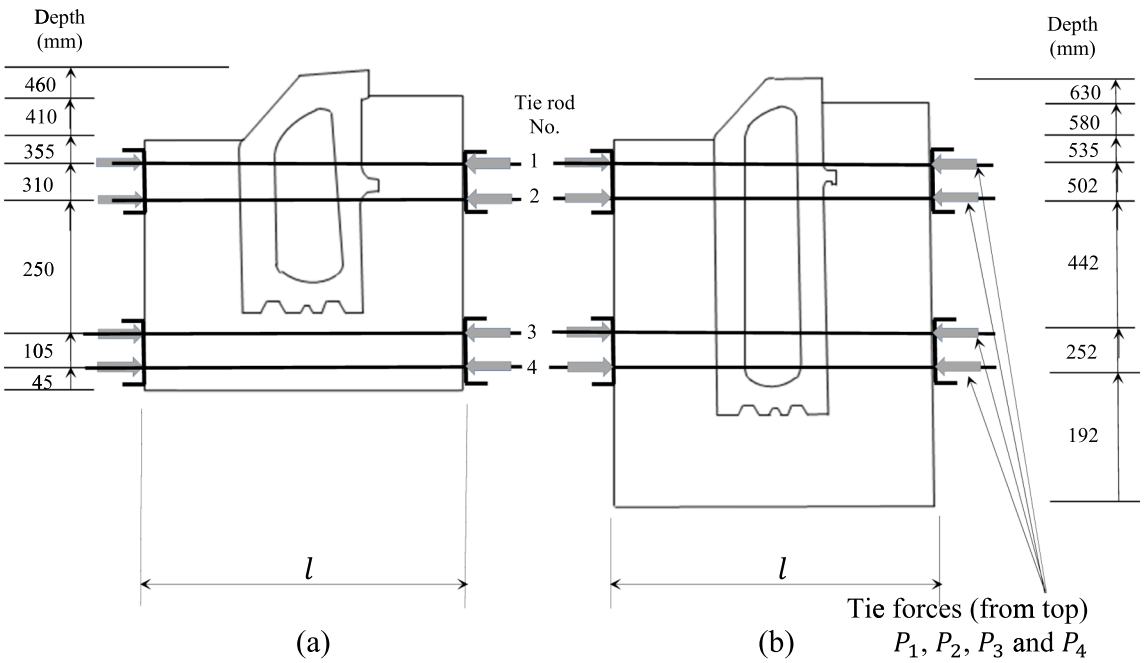

Fig. 4 Locations of threaded tie rods on **a** 305 mm and **b** 480 mm kerbs, not to scale (one end elevation shown e.g. Left (L), similar configuration on opposite end elevation, e.g. Right (R))

by Cromwell Tools, Sheffield, UK. A tensile test was also conducted on two similar tie rods to establish their elastic modulus and yield and ultimate strength properties.

The strain in the threaded tie rods was measured using calibrated vibrating wire strain gauges, supplied by Geosense, Bury St. Edmunds, UK, type VWS-2000 and with a range of 2000 microstrain (Fig. 3). Strain readings were automatically recorded on a datataker DT85. The positions of the tie bars in relation to the base of the drainage kerb assembly are given in Fig. 4.

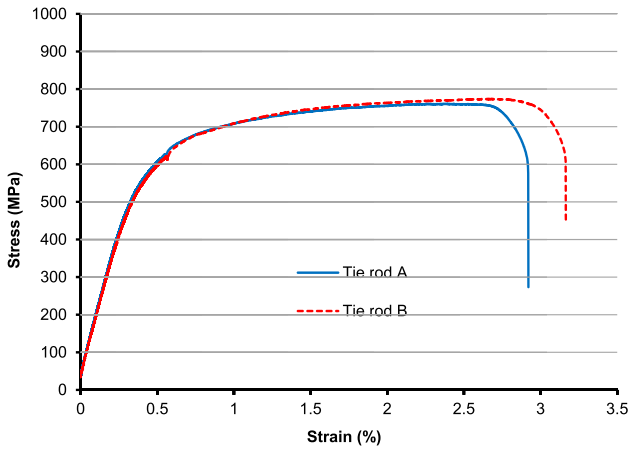

Fig. 5 Stress/strain profiles for as-received threaded tie rods A & B

5 Test results

5.1 Tensile properties of tie bars

The result of the tensile strength tests for the threaded tie rods is given in Fig. 5. Two rods were tested and both show similar performance through the elastic region to yield and beyond. However, Tie rod 1 exhibited slightly lower ductility than Tie rod 2 but it is the performance in the elastic region that is more relevant. The elastic moduli were 177.13 and 171.87 kN/mm^2 for tie rods 1 and 2 respectively giving an average of 174.5 kN/mm^2. Since the 6 mm diameter tie rods were threaded, the root (or minimum) area was taken as 20.1 mm^2 as specified by the suppliers.

5.2 Lateral stress in tie bars

Referring to Fig. 3, four ties rods are shown on each end of the test kerbs. Each end is labelled 'Left' and 'Right'. Figure 4 identifies the tie rod number, starting with No. 1 at the top through to 4 at the bottom. For each kerb size, three specimens were tested, labelled A—C. An example of the measured stresses on the four left and four right tie rods is given in Fig. 6 for one kerb only, kerb 480 (A) and these stress profiles are generally repeated for all kerbs. The peak stress determined for each of the 3 × 480 kerbs and 3 × 305 kerbs are given in Table 1 which were averaged for analytical purposes. Referring to Table 1 the total stress recorded at each tie rod level is presented (Ttl 1–4). Due to slight eccentricities in the loading, the measured stresses varied between the Left and Right tie rods at each level. The maximum stress recorded was 497 N/mm^2 in Tie Rod R_2 in kerb 480 (B) but still in the elastic region if compared to the stress/strain curves in Fig. 5.

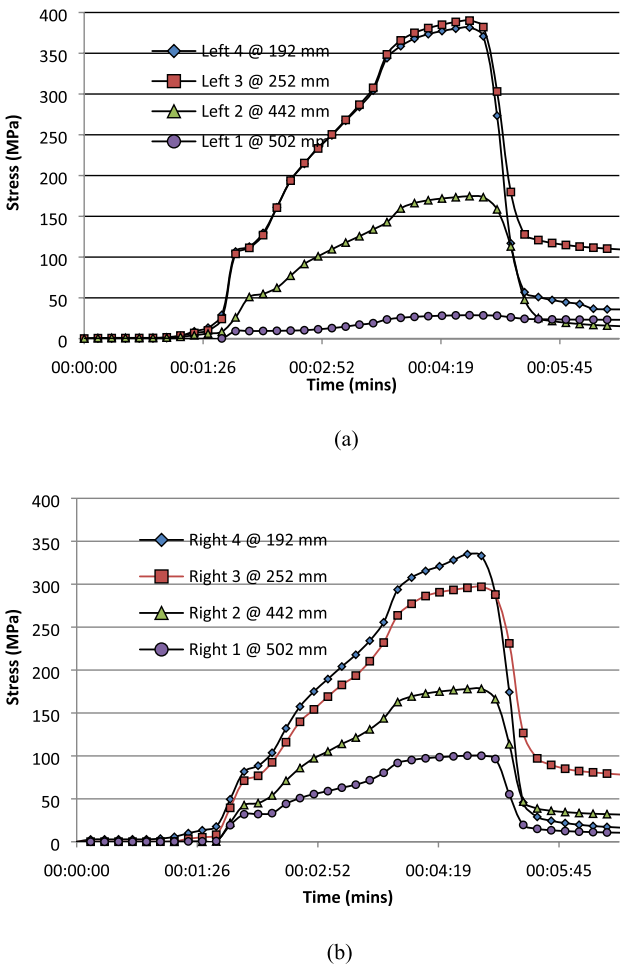

Fig. 6 Measured stress on the **a** Left (L) and **b** Right (R) tie rods for kerb 480 (A)

5.3 Deformation of loaded recycled plastic drainage kerb

The relationship between the total force at each tie rod level (i.e. the sum of both tie rods) and the height of the tie rod levels is given in Fig. 7, along with the approximate positions of the 305 and 480 kerbs in relation to the load points (tie rod locations, including 150 mm of base concrete). Referring to Fig. 7, the line of best fit for both kerbs is in the form of a polynomial meaning that the lateral bursting force imposed is not linear along the depth. The 480 kerb exhibits the largest force, just over 14 kN at a height of about 420 mm from the bottom of the concrete base, near to the location of tie rod 2, see Fig. 7. This is in the vicinity where the maximum bursting effect would be expected i.e. at approximately halfway along the height of the kerb. With regards to the 305 kerb, a maximum bursting force is evident between tie rods 1 and 2, again approximately halfway along the height of the kerb, but

Table 1 Stress in tie rods during D400 loading

Stress (N/mm^2)												
Kerb	L_1	R_1	Ttl 1	L_2	R_2	Ttl 2	L_3	R_3	Ttl 3	L_4	R_4	Ttl 4
305 (A)	251	239	490	256	224	481	82	53	135	1	0	1
305 (B)	270	340	609	253	184	437	90	103	194	1	10	11
305 (C)	333	145	478	375	194	569	97	11	108	10	0	10
Average			526			495			146			7
Distance from base (mm, see Fig. 4a)		45			105			250			310	
480 (A)	382	335	717	390	297	687	175	178	353	29	100	129
480 (B)	313	335	648	360	497	858	268	349	617	127	245	372
480 (C)	231	337	569	244	362	606	121	189	310	1	119	119
Average			644			717			427			207
Distance from base (mm, see Fig. 4b)		192			252			442			502	

Key. L1, L2, L3, L4: Tie rod identifiers on the left-hand side (L) of the drainage system at positions 1–4 (see Fig. 4). R1, R2, R3, R4: Tie rod identifiers on the right-hand side (R) of the drainage system at positions 1–4 (see Fig. 4). Ttl 1, Ttl 2, Ttl 3, Ttl 4: Total strains recorded at each of the four tie rod positions e.g. L1 + R1 = Ttl 1 etc. (A), (B), (C): Identifier for each of the three specimens tested for each kerb size

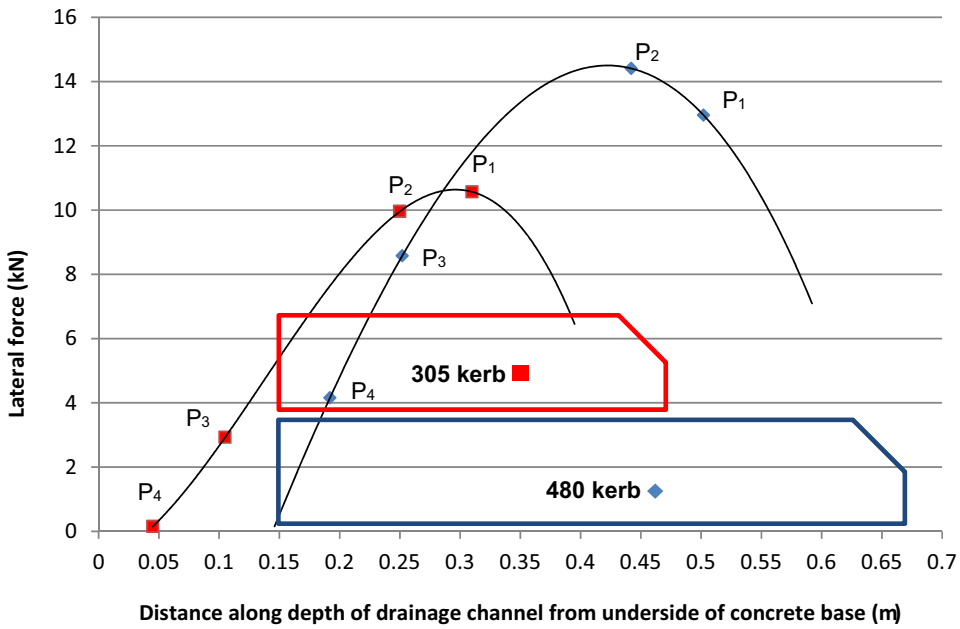

Fig. 7 Relationship between lateral force and depth for kerbs

since the kerb is shorter and stockier than the 480, the magnitude of force is lower, Fig. 7.

6 Determination of tensile stress in the concrete haunches

Referring to Fig. 7, it is clear that the deeper 480 kerb exerts a higher lateral force compared to the shallower 305 kerb, with the peak lateral force at approximately mid-height for both kerbs. This lateral force will induce tensile stress in the concrete haunch which may lead to cracking or failure if sufficiently high. The forces presented at the four locations in Fig. 7 were determined from the strains measured as described in Sect. 4. In order to get an indication of the structural performance of the concrete haunch as a result of the lateral forces, an estimate of the uniformly distributed load (UDL) where the drainage kerb contacts the concrete haunch is required. The forces shown in Fig. 7 are concentrated point loads and need to be transformed

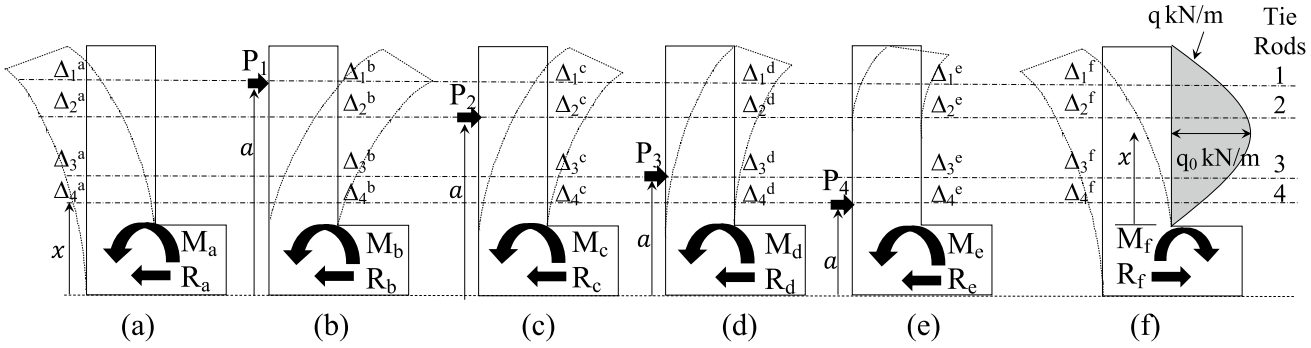

Fig. 8 Determination of approximated peak load q_0 on the cantilever concrete haunch as a result of measured and predicted deflections (480 kerb): **a** resultant positive deflection as measured by the tie rod extensions; **b**–**e** calculated negative deflections due to the tie rod forces; **f** positive deflections due to the distrbuted lateral load q (all deflections shown exaggerated)

into an appropriate UDL to better represent actual conditions. This analysis is explained in greater detail in the following sections in conjunction with Fig. 8. Referring to Fig. 8, six diagrams (a–e) representing the left hand side of the 480 concrete cradle are presented which describe the measured and virtual deflections on the cantilever concrete front haunch as a result of the loading applied as described in Sect. 4.

Figure 8a represents the measured extensions at the four tie rod locations with deflections Δ_1^a–Δ_4^a (see also Fig. 4). In general terms, these measured deflections are the net result of the combined negative deflections produced by the opposing tie rod forces and the positive deflections due to the bursting force. Horizontal reaction R_a and bending moment M_a will also be present at the support. This is analysed in Sect. 6.1. Referring to Fig. 3, it is clear that the instrumented four tie rods also provide a reaction against excessive outward deflection of the front and rear concrete haunches. Therefore, the tie rods offer a reaction against outward movement of the front and rear concrete haunches at locations 1–4 (see Fig. 4), the magnitude of which are similar to the forces given in Fig. 7. Figure 8b–e shows the deflections at the four tie rod locations as a result of isolating each of the reactions P_1–P_4. Referring to Fig. 8b, Reaction P_1 can be assumed to act as a point load on the cantilever haunch leading to deflections Δ_1^b—Δ_4^b at the four tie rod locations. The fixed end of the cantilever exhibits both a horizontal reaction R_b and bending moment M_b for equilibrium. Standard equations for the deflection of a cantilever beam will be used to determine the deflections of the cantilever haunch at this point. This is repeated for reactions P_2, P_3 and P_4 as shown in Fig. 8c–e. The analysis is presented in Sect. 6.2.

Referring to Fig. 7, it is clear that the bursting force is not uniform along the depth of the drainage kerb with a higher magnitude of force present towards the mid-depth of the concrete haunch with lower bursting forces evident towards the free and fixed-ends of the concrete haunch. In order to establish an equivalent bursting load acting on the cantilever concrete haunch, it is assumed for simplicity that the bursting load tending to push the haunches outwards is in the form of a parabolic load as shown in Fig. 8f with a horizontal reaction and bending moment at the support also as shown in Fig. 8f. This load has a varying intensity of q kN/m and a peak intensity of q_0 (kN/m) at mid-depth. An equation for the deflection of the simulated parabolic load in terms of q_0 is developed in Sect. 6.3. However, the value of q_0 is unknown but the extension of the tie rods from strain measurements (Fig. 8a) and the defection of the concrete cantilever at the tie rod locations as a result of the simulated loads P_1 to P_4 from standard equations (Fig. 8b–e) are known so these are used to obtain q_0. Therefore, the deflections as a result of the loads shown in Fig. 8a–f will be algebraically added together at each tie rod location to enable an estimate of the peak load, q_0 to be determined. Therefore, for example at tie rod location 1, the equation is

$$\Delta_{1\,measured} = \Delta_{1\,q0} - \sum(\Delta_{P1} + \Delta_{P2} + \Delta_{P3} + \Delta_{P4}) \quad (1)$$

This is repeated for other tie rod locations 2, 3 and 4 and all should yield a similar value for q_0. The detailed analysis is given in Sect. 6.4

6.1 Measured lateral extensions on the tie rods

The vibrating wire gauges in Fig. 4 measure the strain in the tie rods using the equation supplied by the manufacturer:

$$\varepsilon = (F_1^2 - F_2^2)(GF)(B) \quad (2)$$

where ε is the strain, F_1 is the datum frequency of the wire, F_2 is the subsequent frequency, GF is the Gauge Factor

(3.718) and *B* is the Batch Number (0.958) (GF and B are constants provided by the manufacturer during calibration prior to shipping the strain gauges). The strain determined from Eq. 2 in the analysis was the maximum recorded i.e. when the load of 400 kN was applied onto the drainage kerb assembly and held for 30 s. Hence, the extension of Tie Rod 1 was determined using Eq. 3 (modified from strain = change in length/original length) where *l* is the length of the threaded rods (taken from the anchor points on the inner face of the webs of the channel sections) as shown in Fig. 4:

$$\Delta_1^a = \varepsilon_1 l \tag{3}$$

This was repeated for tie rod locations 2, 3 and 4 giving Δ_2^a, Δ_3^a and Δ_4^a. For equilibrium, a horizontal reaction R_a and bending moment M_a will also be present at the support as shown in Fig. 8a.

6.2 Deflection of concrete haunch due to virtual reactions P_1, P_2, P_3 and P_4

The four forces in the tie rods (P_1, P_2, P_3 and P_4) can be considered as virtual loads on the cantilever beam. Each reaction can be considered in turn to cause a virtual deflection in the beam and standard cantilever beam deflection equations are used for this purpose. Referring to Fig. 8b for load P_1, the deflection Δ at any distance *x* can be obtained when $0 \le x \le a$ from [25]

$$\Delta = \frac{P_1 x^2}{6EI}(3a - x) \tag{4}$$

where *a* is the distance to the reaction and *x* is the distance to the four tie rod locations, both measured from the base. However, when $a \le x \le L$, the deflection Δ is obtained from

$$\Delta = \frac{P_1 a^2}{6EI}(3x - a) \tag{5}$$

Therefore, the deflections at the four tie rod locations Δ_1^b, Δ_2^b, Δ_3^b and Δ_4^b can be obtained from Eq. 4, 5 as a result of the virtual load due to reaction P_1. This is repeated for reactions P_2, P_3 and P_4 giving the corresponding deflections at the four tie rod locations, Fig. 8c–e. However, for analytical purposes, the deflection from only one reaction (P_1, P_2, P_3 or P_4) is required but all four were obtained regardless as a cross check. However, accuracy can be an issue where the measured extensions are very low i.e. P_3 or P_4 near the cantilever support and this will be considered in Sect. 6.4.

6.3 Development of deflection equation for the peak parabolic load, q_0

Referring to Fig. 8f, since the load is in the form of a parabolic curve, the load *q* can be written in the form of a quadratic equation, namely

$$q = ax^2 + bx + c \tag{6}$$

Referring to Eq. 6, values for *a*, *b* and *c* are required. Therefore, $q = 0$ at $x = 0$ where *x* is measured from the top of the concrete base so takes into account the portion of the concrete influenced by the load *q*. Therefore, substituting this into Eq. 6 gives

$$c = 0 \tag{7}$$

Also, $q = 0$ at $x = L$ and substituting into Eq. 6 gives

$$0 = aL^2 + bL \tag{8}$$

Simplifying Eq. 8 gives

$$b = -aL \tag{9}$$

The load intensity $q = q_0$ (peak load) at $x = \frac{L}{2}$. Again, substituting this into Eq. 6 gives

$$q_0 = \frac{aL^2}{4} + \frac{bL}{2} \tag{10}$$

But since $b = -aL$ from Eq. 9, 10 can be written as

$$q_0 = \frac{aL^2}{4} - \frac{aL^2}{2} \tag{11}$$

Simplifying Eq. 11 gives

$$q_0 = -\frac{aL^2}{4} \tag{12}$$

Rearranging Eq. 12 in terms of *a* gives

$$a = -\frac{4q_0}{L^2} \tag{13}$$

but since $b = -aL$ from Eq. 9,

$$b = \frac{4q_0}{L} \tag{14}$$

Substituting Eq. 13, 14 into Eq. 6 and simplifying gives an expression for the load intensity *q* as a result of the bursting load from the deforming kerb on the cantilever haunch of the concrete cradle

$$q = \frac{4q_0}{L}\left(-\frac{x^2}{L} + x\right) \tag{15}$$

The load *q* acting on the concrete haunch can also be expressed as

$$EI\frac{d^4w}{dx^4} = q \tag{16}$$

Inserting Eq. 15 into Eq. 16 gives

$$EI\frac{d^4w}{dx^4} = \frac{4q_0}{L}(-\frac{x^2}{L} + x) \tag{17}$$

Integrating Eq. 17 gives an expression for the shear

$$EI\frac{d^3w}{dx^3} = \frac{4q_0}{L}\left(-\frac{x^3}{3L} + \frac{x^2}{2}\right) + C_1 \tag{18}$$

Since $EI\frac{d^3w}{dx^3} = 0$ at $x = L$, therefore, from Eq. 18

$$0 = \frac{4q_0}{L}\left(-\frac{L^3}{3L} + \frac{L^2}{2}\right) + C_1 \tag{19}$$

Simplifying Eq. 19 gives

$$C_1 = -\frac{2q_0L}{3} \tag{20}$$

Substituting Eq. 20 into Eq. 18 gives

$$EI\frac{d^3w}{dx^3} = \frac{4q_0}{L}\left(-\frac{x^3}{3L} + \frac{x^2}{2}\right) - \frac{2q_0L}{3} \tag{21}$$

Integrating Eq. 21 gives an expression for the moment

$$EI\frac{d^2w}{dx^2} = \frac{4q_0}{L}\left(-\frac{x^4}{12L} + \frac{x^3}{6}\right) - \frac{2q_0Lx}{3} + C_2 \tag{22}$$

Since $EI\frac{d^2w}{dx^2} = 0$ at $x = L$, therefore

$$0 = \frac{4q_0}{L}\left(-\frac{L^4}{12L} + \frac{L^3}{6}\right) - \frac{2q_0L^2}{3} + C_2 \tag{23}$$

Simplifying Eq. 23 gives

$$C_2 = \frac{q_0L^2}{3} \tag{24}$$

Substituting Eq. 24 into Eq. 22 gives

$$EI\frac{d^2w}{dx^2} = \frac{4q_0}{L}\left(-\frac{x^4}{12L} + \frac{x^3}{6}\right) - \frac{2q_0Lx}{3} + \frac{q_0L^2}{3} \tag{25}$$

Integrating Eq. 25 gives an expression for the slope

$$EI\frac{dw}{dx} = \frac{4q_0}{L}\left(-\frac{x^5}{60L} + \frac{x^4}{24}\right) - \frac{2q_0Lx^2}{6} + \frac{q_0L^2x}{3} + C_3 \tag{26}$$

However, $EI\frac{dw}{dx} = 0$ at $x = 0$, therefore

$$C_3 = 0 \tag{27}$$

Finally, integrating Eq. 27 gives

$$EIw = \frac{4q_0}{L}\left(-\frac{x^6}{360L} + \frac{x^5}{120}\right) - \frac{2q_0Lx^3}{18} + \frac{q_0L^2x^2}{6} + C_4 \tag{28}$$

But since $EIw = 0$ at $x = 0$, therefore

$$C_4 = 0 \tag{29}$$

Simplifying Eq. 28 gives an expression for the deflection of the parabolic load on the concrete cantilever haunch as shown in Fig. 8 (f)

$$w = q_0\left(\frac{x^5}{45L} - \frac{Lx^3}{9} + \frac{L^2x^2}{6}\right)/EI \tag{30}$$

where E was taken as E_{cm} from

$$E_{cm} = 22[\frac{f_{cm}}{10}]^{0.3} \tag{31}$$

from Table 3.1 in EC 2 [7] (f_{cm}=f_{ck} + 8, f_{ck} being the concrete cylinder strength) and $I = bd^3/12$ (b = 500 mm and d = 150 mm).

6.4 Determination of simulated peak load, q_0

Referring to Fig. 8, the extension in any one of the four tie bars (see Fig. 8a), labelled $\Delta_1{}^a$–$\Delta_4{}^a$ must be equal to the deflection caused at the corresponding location as a result of the simulated load with peak intensity q_0 minus the deformation in the corresponding tie rods locations from the Reactions P_1–P_4 as shown in Fig. 8b–e. This was given in Eq. 1. Since four positions on the concrete haunch have been considered for analysis to coincide with the location of the tie rods, then four independent deflection equations can be established to determine the unknown value of the peak load q_0 (each equation should yield the same value of q_0 so considering four equations allows an average to be obtained). Therefore, rearranging Eq. 1 and inserting appropriate terms for tie rod level 1 in Fig. 8 gives:

$$\Delta_1^a + \sum(\Delta_1^b + \Delta_1^c + \Delta_1^d + \Delta_1^e) = \Delta_1^f q_0 \tag{32}$$

Similarly, deflection equations for tie rod levels 2–4 can also be established as follows:

$$\Delta_2^a + \sum(\Delta_2^b + \Delta_2^c + \Delta_2^d + \Delta_2^e) = \Delta_2^f q_0 \tag{33}$$

$$\Delta_3^a + \sum(\Delta_3^b + \Delta_3^c + \Delta_3^d + \Delta_3^e) = \Delta_3^f q_0 \tag{34}$$

$$\Delta_4^a + \sum(\Delta_4^b + \Delta_4^c + \Delta_4^d + \Delta_4^e) = \Delta_4^f q_0 \tag{35}$$

Therefore Eqs. 32, 33, 34, 35 are used to calculate four different values for peak load q_0. Referring to Table 2, the

Table 2 Determination of peak load q_0

1	2	3	4	5	6	7
			480 mm drainage kerb		305 mm drainage kerb	
Haunch, see	Deflections via:	Deflections calculated via:	Deflections (m) (Front Haunch)	q_0(kN/m) (Front Haunch)	Deflections (m)	q_0(kN/m) (Front Haunch)
Figure 8a	Strain gauges	Equation 3	$\Delta_1^a = 8.22\times10^{-4}$ $\Delta_2^a = 9.14\times10^{-4}$ $\Delta_3^a = 5.44\times10^{-4}$ $\Delta_4^a = 2.64\times10^{-4}$	–	$\Delta_1^a = 6.93\times10^{-4}$ $\Delta_2^a = 6.53\times10^{-4}$ $\Delta_3^a = 1.92\times10^{-4}$ $\Delta_4^a = 9.88\times10^{-6}$	–
Figure 8b	Reaction $P_1 = 12.95$ kN at tie rod locations 1–4	Equation 4 or Eq. 5	$\Delta_1^b = 1.32\times10^{-4}$ $\Delta_2^b = 1.09\times10^{-4}$ $\Delta_3^b = 4.16\times10^{-5}$ $\Delta_4^b = 2.53\times10^{-5}$	–	$\Delta_1^b = 3.11\times10^{-5}$ $\Delta_2^b = 2.22\times10^{-5}$ $\Delta_3^b = 4.75\times10^{-6}$ $\Delta_4^b = 9.36\times10^{-7}$	–
Figure 8c	Reaction $P_2 = 14.41$ kN at tie rod locations 1–4	Equation 4 or Eq. 5	$\Delta_1^c = 1.21\times10^{-4}$ $\Delta_2^c = 1.00\times10^{-4}$ $\Delta_3^c = 3.96\times10^{-5}$ $\Delta_4^c = 2.43\times10^{-5}$	–	$\Delta_1^c = 2.47\times10^{-5}$ $\Delta_2^c = 1.82\times10^{-5}$ $\Delta_3^c = 4.13\times10^{-6}$ $\Delta_4^c = 8.29\times10^{-7}$	–
Figure 8d	Reaction $P_3 = 8.58$ kN at tie rod locations 1–4	Equation 4 or Eq. 5	$\Delta_1^d = 2.75\times10^{-5}$ $\Delta_2^d = 2.36\times10^{-5}$ $\Delta_3^d = 1.11\times10^{-5}$ $\Delta_4^d = 7.19\times10^{-6}$	–	$\Delta_1^d = 3.14\times10^{-6}$ $\Delta_2^d = 2.46\times10^{-6}$ $\Delta_3^d = 8.01\times10^{-7}$ $\Delta_4^d = 1.89\times10^{-7}$	–
Figure 8e	Reaction $P_4 = 4.16$ kN at tie rod locations 1–4	Equation 4 or Eq. 5	$\Delta_1^e = 8.12\times10^{-6}$ $\Delta_2^e = 7.01\times10^{-6}$ $\Delta_3^e = 3.48\times10^{-6}$ $\Delta_4^e = 2.37\times10^{-6}$	-	$\Delta_1^e = 3.00\times10^{-7}$ $\Delta_2^e = 2.39\times10^{-7}$ $\Delta_3^e = 9.16\times10^{-8}$ $\Delta_4^e = 3.05\times10^{-8}$	–
Figure 8f	Simulated lateral peak load q_0	Equation 30	$\Delta_1^f = 1.41\times10^{-6}\, q_0$ $\Delta_2^f = 1.19\times10^{-6}\, q_0$ $\Delta_3^f = 5.10\times10^{-7}\, q_0$ $\Delta_4^f = 3.19\times10^{-7}\, q_0$	786 (Eq. 32) 966 (Eq. 33) 1256 (Eq. 34) 1013 (Eq. 35) Average: 876 (Δ_1^f, Δ_2^f)	$\Delta_1^f = 2.38\times10^{-7}\, q_0$ $\Delta_2^f = 1.75\times10^{-7}\, q_0$ $\Delta_3^f = 3.96\times10^{-8}\, q_0$ $\Delta_4^f = 7.95\times10^{-9}\, q_0$	3161 (Eq. 32) 3983 (Eq. 33) 5086 (Eq. 34) 1493 (Eq. 35) Average: 3572 (Δ_1^f, Δ_2^f)

deflections for the front haunch only for the 480 and 305 kerbs are given (a similar analysis was also done for the rear haunches and the magnitude of peak load q_0 was obtained but are omitted from Table 2 due to space limitations). In Table 2, col. 1, the deflections as a result of the applied load are related to one of the diagrams in Fig. 8a–e with further descriptions given in col. 2. The equations used to calculate the deflections are given in col. 3 followed by the actual deflections for the 480 kerb in col. 4. Four slightly different values for peak load q_0 are given in col. 5 for the 480 kerb, ranging between 786 and 1256 kN/m. The deflections for the 305 kerb and corresponding peak load q_0 are given in cols. 6 and 7 (average 3572 kN/m for tie rods 1 and 2). Due to the very small deflections either measured or calculated in this analysis, it is perhaps too much to expect closer agreement for peak load q_0 values, especially for deflections at tie rod levels 3 and 4 where small errors in readings can give a high percentage difference. Referring to Fig. 4a, tie rod locations for the 305 kerb are within the base concrete and so will be influenced by the resistance given by the concrete. Therefore, the analysis of tie rods 3 and 4 are best excluded on the grounds of unreliable readings and for consistency, the same two tie rods for the 480 kerb will also be excluded meaning only tie rods locations 1 and 2 will be used and this is shown in Table 2, cols. 4 and 6. It was mentioned in Sect. 6.2 that the finding from only one tie rod is theoretically required but for greater accuracy, the average from tie rods 1 and 2 is used in the analysis.

6.5 Determination of resultant load, Q

Referring to Fig. 8f, the parabolic load which represents the lateral load on the front concrete haunch as a result of deformation in the drainage kerb is denoted q whereas the peak load is denoted q_0. An expression for the load q is given in Eq. 15. The peak load q_0 was determined in Sect. 6.4. To enable a simplified prediction of the maximum tensile stress in the concrete haunch to be determined, the expression for the uniform load q (Eq. 15) can be integrated to give the resultant force Q acting on the front concrete haunch. Therefore

$$Q = \int_0^L q dx \tag{36}$$

Substituting Eq. 15 into Eq. 36 gives

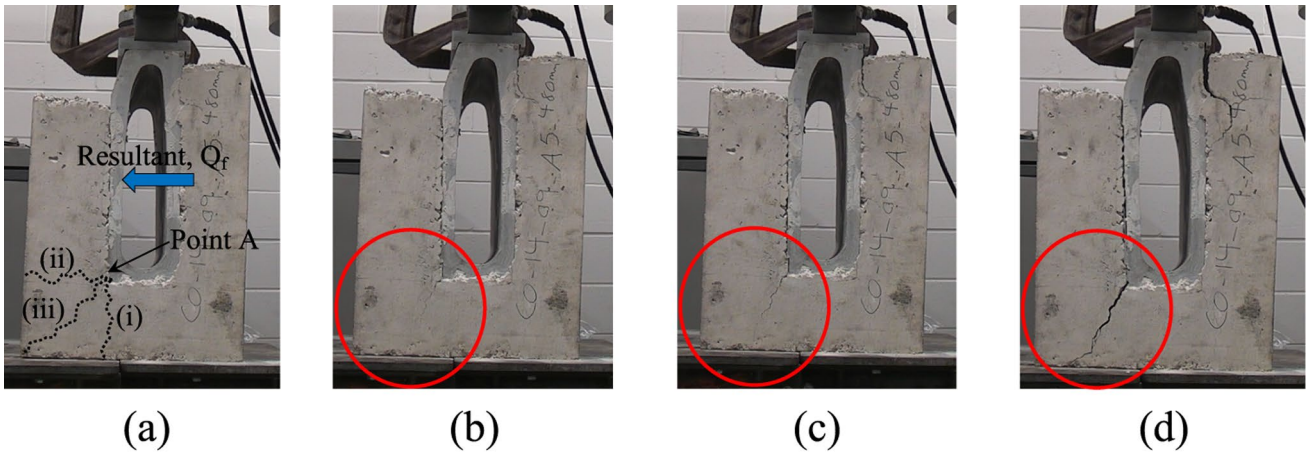

Fig. 9 Crack propagation at front haunch due to increasing lateral force

$$Q = \int_0^L \frac{4q_0}{L}(-\frac{x^2}{L} + x)dx \tag{37}$$

Integrating Eq. 37 gives

$$Q = \frac{4q_0}{L}\left[(-\frac{x^3}{3L} + \frac{x^2}{2})\right]_0^L \tag{38}$$

Replacing x with the boundary values L and 0 in Eq. 38 and simplifying gives

$$Q = \frac{4q_0}{L}(-\frac{L^2}{3} + \frac{L^2}{2}) \tag{39}$$

Simplifying Eq. 39 gives the expression for the total load Q acting on the concrete haunch

$$Q = \frac{2q_0L}{3} \tag{40}$$

The term Q in this analysis is subscripted with f (for front) and r (for rear) giving resultant forces Q_f and Q_r respectively.

6.6 Determination of failure mode in the concrete haunch

Referring to Fig. 9, when the kerb is loaded in accordance with the test standard, cracking, if present, will initiate at Point A on either the front or rear haunch, at the intersection between the concrete base and cantilever as this will be the tensile face as a result of lateral loading. The magnitude of this tensile stress could cause cracking and failure of the concrete surround if the induced stresses are greater than the flexural strength of the concrete. However, in reality, the kerb and concrete surround is restrained by the haunch construction to the front and rear. A carriageway or other hard wearing course (e.g. car park) is normally constructed at the front, the rear construction may vary with materials of varying stiffness, for example, footpath for pedestrian access or simple landscaping where access is not required, for example on a roundabout where vegetation or similar is provided for aesthetic purposes.

A representation of the effect of the resultant force, Q_f, acting on the concrete cantilever (front haunch) is given in Fig. 9. The type of failure mode will reveal how the concrete haunch acts under the action of the resultant force, Q_f. This can be done via investigating the orientation of the crack as shown in Fig. 9a. Three possible simplified types of crack orientations are given initiating from the intersection Point A, in the case of this example, the front haunch since the resultant Q_f was greater than Q_r, the resultant in the rear haunch. Crack Type (i) is predominantly vertical and at right angles to the line of action of the resultant force Q_f, meaning a tension failure results (the haunch splits from the concrete cradle under a sliding type of action). Crack Type (ii) is parallel to the line of action of the resultant force Q_f meaning it is flexural as the crack propagates as a result of bending action. Finally, Crack Type (iii) is at an angle from Point A meaning it is as a result of both bending and flexural and if present in equal measures, the line of the crack would roughly be at 45°.

Figure 9b–d shows the failure sequence from a previous load test on a similar kerb (480 mm deep) but without the restraint provided by the threaded bars. The crack initiates at Point A as shown in Fig. 9b, c and propagates predominantly downwards at a shallow angle to the vertical until the front concrete haunch completely splits from the base concrete as the tensile stress exerted is greater than the tensile strength of the concrete (Fig. 9d). The orientation of the crack, therefore, is between Crack (i) and Crack (ii) in Fig. 9a meaning failure is as a result of pure tension being developed in the concrete in addition to some flexure as the front haunch splits from the base concrete.

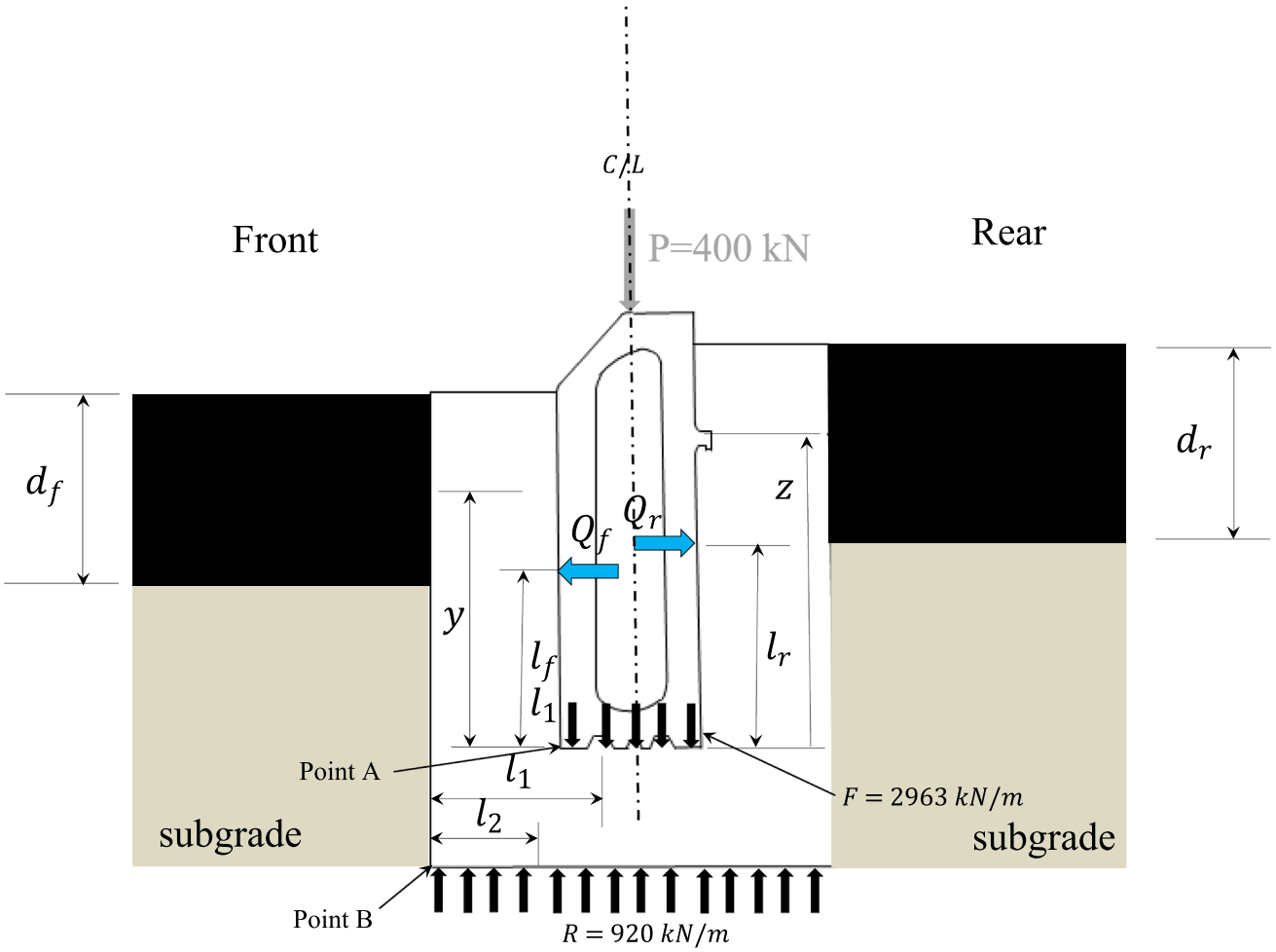

Fig. 10 Load exerted laterally for 480 kerb

6.7 Determination of the reaction in the pavement construction

In the UK, a pavement is designed in accordance with HA documentation [21] and is (predominantly) flexible or rigid. In flexible pavement construction, there is usually a well prepared subgrade with one layer (or more) of unbound base material topped with a layer of bituminous hot mix asphalt. Asphalt on a high volume flexible pavement (≥80 million standard axles (msa)) is laid at a minimum depth of 180 mm meaning that the top 180 mm of the submerged kerb is supported by asphalt (plus the surround concrete).

The resultant of the udl (Q_f) acting on the front cantilever was found from Eq. 40 and is shown in Fig. 10 which also shows the depth of asphalt and subgrade. The force acting on the rear cantilever (Q_r) can also be found using the same equation. Concentrating on the front cantilever, the resultant force (Q_f) will exert a tensile stress in the concrete and if this stress is greater than the tensile stress in the concrete, then cracking will occur. The concrete surround is Grade C20 but actual cube strength was 23 MPa (equivalent to a cylinder strength of 18.4 MPa [26]) at the time of testing, Sect. 3. Using Table 3.1 from EC 2 [27] gives a tensile strength of

$$f_{ctm} = (0.3)(f_{ck}^{2/3})MPa \tag{41}$$

Which gives $f_{ctm} = 2.10$ MPa. However, as is normally the case for concrete materials in design, a factor of safety, $\gamma = 1.5$ (e.g. from Eurocode 2 [27]) is used meaning the factored strength ($f_{ctm(fact)}$) is 1.39 MPa.

In the laboratory testing, a single kerb assembly was tested. In field applications, the recycled drainage kerbs are joined to one another using a high performance one-part polyurethane sealant and butted together meaning there is a continuous line of kerbs with a certain amount of restraint provided which is absent in the laboratory tests. In this analysis, it is assumed that due to the continuity, the combined resistance given by two kerbs is assumed, that being either half a kerb either side of the impacted kerb or a full kerb either side of the line of adhesion if impact is on the joint.

Table 3 Determination of lateral forces

Force/reaction	480 kerb			305 kerb		
	q_0(kN/m)	Value (kN)	Total (kN)	q_0(kN/m)	Value (kN)	Total (kN)
R_f	–	139.4 (Eq. 42)	341.7	–	408.5 (Eq. 42)	825.8
Q_r	876 (Sect. 6.4)	202.3 (Eq. 40)		3572 (Sect. 6.4)	417.3 (Eq. 40)	
R_r	–	120.2 (Eq. 42)	345.1	–	318.4 (Eq. 42)	806.5
Q_f	706 (Sect. 6.4)	224.9 (Eq. 40)		2408 (Sect. 6.4)	488.1 (Eq. 40)	
		$\Delta \sum F_H$	3.3		$\Delta \sum F_H$	19.3

For the front haunch of the 480 kerb, $q_0 = 876$ kN/m and $L = 0.385$ m and substituting these into Eq. 40 gives $Q_f = 224.9$ kN. The rear haunch was also assumed to consist of an asphalt layer of similar depth for calculation purposes but this construction detail may vary greatly across different schemes in reality, ranging from an asphalt footpath to well compacted dense soil, for example on a roundabout. Q_r for the rear haunch was also calculated with appropriate values inserted into Eq. 40 giving $Q_r = 202.3$ kN.

It is assumed that the asphalt on the front haunch (Fig. 10) will provide a reaction, R_f to the lateral resultant Q_f and acts at mid-depth of the asphalt ($\frac{d_p}{2} = 90mm$).

Referring to Fig. 10 and considering the front haunch only (left hand side), summing the moments about Point B ($\sum M_B = 0$) gives

$$(R_f)(y + 0.150) + \left(\frac{F}{2}\right)(l_1) - (Q_f)(l_f + 0.150) - \left(\frac{R}{2}\right)(l_2) = 0 \tag{42}$$

where 0.150 is the concrete thickness (m). Substituting known values into Eq. 42 gives a value for R_f which for the front haunch of the 480 kerb was 139.4 kN. A similar calculation was done for the right-hand side of Fig. 10 (rear haunch) and R_r was 120.2 kN. Since Q_f and Q_r are already known from Eq. 40, a check can be conducted for horizontal equilibrium. Therefore, summing the forces horizontally (see Fig. 10) gives

$$R_f + Q_r = R_r + Q_f \tag{43}$$

or

$$139.4 + 202.3 = 120.2 + 224.9 \tag{44}$$

or 341.7 kN versus 345.1 kN which is a very satisfactory correlation. A similar calculation was done for the 305 kerb and exhibited total forces of 825.8 kN versus 806.5 kN, a higher difference of 19.3 kN (~ 2.4%) but is considered reasonable under the circumstances. A summary of the key values are given in Table 3.

It was shown in Fig. 9a that cracking initiated at Point A for unsupported drainage kerbs assemblies. Therefore, the bending moment at this point can be calculated from

$$M = (R_f)(y) - (Q_f)(l_f) = 0 \tag{45}$$

giving

$$M = (139.4)(0.295) - (224.9)(0.193) = 2.28kNm \tag{46}$$

The applied stress at Point A in Fig. 10 can be calculated, with the assumption that two kerbs are fully bonded to each other and act in tandem to carry to applied forces as described above. Therefore

$$f = \frac{(M)(y)}{I} + \frac{Q_f - R_f}{A} \tag{47}$$

Substituting known values into Eq. 47 gives

$$f = \frac{(2.28)(10^6)(\frac{150}{2})}{(1000)(150^3)(\frac{1}{12})} + \frac{(224.9 - 139.4)(10^3)}{(1000)(150)} \tag{48}$$

or $f = 1.18$ MPa. Comparing this applied stress in the concrete to the factored tensile strength of the concrete ($f_{ctm(fact)} = 1.39$ MPa) means the concrete remains crack free. In addition, irrespective of the construction material used on the rear and front haunch, the applied stress is very low. For example, the reaction R_f (139.4 kN), despite being assumed to be provided by only 180 mm of asphalt, would induces a stress of only 0.77 MPa [$(139.4)(10^3)/(1000)(180)$]. For the 305 kerb, a maximum stress of 2.3 MPa would be present in the asphalt in the front haunch.

7 Discussion of results

The recycled kerbs were tested in accordance with BS EN 1533 [19] which applies a vertical load of 400 kN (Class D400) on the kerb. In reality, when any type of road kerb is impacted in-situ, the wheel load will either hit the kerb horizontally or hit and mount the kerb. This loading is different to the type of loading applied under idealised conditions in the laboratory. A 'standard axle' in the UK [28] is defined as an axle exerting or applying a force of 80 kN or 40 kN per wheel (when one wheel is acting on the kerb, the other wheel on the same axel will also provide a downward force on the asphalt to one side of the kerb thereby increasing the restraint). However, the load applied in the laboratory is 40 Te (or 400 kN) meaning the laboratory load is factored upwards by a factor of 10 to account for the dynamic effects of the wheel load. Clearly, in an idealised

laboratory test, there exists the opportunity to perfectly align the kerb in the concrete cradle ensuring they are vertical without tilting in any direction using whereas in-situ, they are placed by hand without any props. In addition, the recycled drainage kerbs in-situ are joined to one another using a high performance one-part polyurethane sealant and butted together meaning there is a continuous line of kerbs with a certain amount of restraint provided which is absent in the laboratory tests. The failure mode in the laboratory testing was akin to mainly tensile and flexural stress as the unsupported front haunch split from the base concrete as a result of the bursting force (tie rods were eliminated in these tests). The whole drainage kerb assembly also rests on a solid bed during application of the load. This, too, may have an influence on the failure mode. For example, referring to Fig. 9, the failure mode was predominantly one of splitting as evidenced by the direction of the crack. However, the steel bed of the test frame provides a reaction at the bottom corner of the concrete cradle (Point B, Fig. 10) meaning the front haunch is unable to bend to cause a flexural failure, especially as it is held down by a vertical load of 400 kN. There is also the possibility that the haunch is so small in length that pure bending action is limited. There may be a certain amount of elasticity in the natural foundation in-situ meaning flexural failure may be more prominent as opposed to splitting (tension failure). However, the key characteristic in the resistance to cracking is the tensile strength on the concrete which is low regardless of whether the pure tensile strength or flexural strength is used in the analysis. Furthermore, the drainage kerb has deemed to pass the test as long as it is able to carry the D400 load and this was the case for all restrained drainage kerbs tested in the laboratory (total of six). The analysis presented in this paper looks to understand the distribution of forces across the drainage kerb assembly which were then used to predict the level of restraint required by the road construction materials. Clearly the results presented in this paper are confined to the drainage kerbs tested under laboratory conditions and give a good indication of the level of restraint required to confine the kerbs in haunch construction materials. The research could be used as a stepping-stone to provide further recommendations to BS EN 1433 [19] to ensure the test standard fully encompasses all drainage kerb materials for road infrastructure projects, either concrete or recycled plastic.

8 Conclusions

The following are the conclusions emanating from the laboratory based load testing of recycled plastic drainage kerbs in accordance with BS EN 1433 [19]. The aim is to determine the level of lateral force exerted as a result of deformation of the drainage kerb under load meaning recycled plastic drainage kerbs can be rigorously assessed in the laboratory to ensure they are fit-for-purpose in the field. The main issue with recycled plastic drainage kerbs is that the vertical test load of 400 kN produces an outward (lateral) bursting force which is likely to lead to cracking of the concrete surround if it is unsupported at the front and rear haunches due to the level of tensile stress generated in the concrete. The highest lateral force recorded is approximately at mid-height along the depth of the kerb, irrespective of kerb size. The strain measuring device monitored the strain at four locations along the depth of the concrete haunch and it proved to be a reliable method. These strains were converted to both deflections (extensions) and forces, the latter being used with standard equations for the deflection of cantilever beams to also establish deflections at the four measuring points. A parabolic bursting force was assumed to act on the concrete haunch with a peak intensity of q_0. By equating this to the resistance to deflection equations, the total lateral bursting force Q was determined on both the front and rear haunch (Q_f and Q_r). The tensile capacity in the concrete section resisting the lateral force was determined and shows that additional support is required from the adjacent construction to both the front and rear haunches of the drainage kerb. The compressive stresses in the adjacent haunch construction materials as a result of the lateral bursting forces are calculable and are shown to be low enough to be safely carried by the materials.

The test method has been shown to be a reliable way of estimating the level of restraint required for loaded recycled plastic drainage kerbs tested under laboratory conditions in accordance with BS EN 1433 [19]. The rigorous analysis conducted in the research has the potential to add significant value to the current test standard [19] with regards to testing recycled plastic drainage kerbs.

Acknowledgements The support from Centre for Infrastructure Management colleagues at Sheffield Hallam University during the laboratory testing is acknowledged.

Compliance with ethical standards

Conflicts of interest The authors' declare they have no conflicts of interest or competing interests.

References

1. Bust PD, Gibb AGF, Haslam RA (2005) Manual handling of highway kerbs-focus group findings. Appl Ergon 36:417–425. https://doi.org/10.1016/j.apergo.2004.05.005
2. Agyeman S, Obeng-Ahenkora NK, Assiamah S, Twumasi G (2019) Exploiting recycled plastic waste as an alternative binder for paving blocks production. Case Stud Con Mats 11:e00246. https://doi.org/10.1016/j.cscm.2019.e00246
3. Ghuge J, Surale S, Patil BM, Bhutekar SB (2019) Utilization of Waste Plastic in Manufacturing of Paver Blocks. Int Res J Eng Tech (IRJET) 6(4):2395–0072
4. Ahmad NFA, Razali SNM, Sahat S, Masiri K (2019) application of polyethylene terephthalate concrete as paver block. J Comp Theor Nanosci 16(12):4960–4964. https://doi.org/10.1166/jctn.2019.8548
5. Shanmugavalli B, Gowtham K, Nalwin PJ, Moorthy BE (2017) Reuse of plastic waste in paver blocks. Int J Eng Res Tech 6(2):2278–0181
6. Hemalatha D (2019) Reuse of waste plastics and demolition waste in the development of plastic paver block, reuse of waste plastics and demolition waste in the development of plastic paver block. J Sci Ind Res 78:248–250
7. Naji AJ, Al-Yousefi HA, Mousa MA, Hussein MJ (2019) Optimization of water-cement ratio in concrete contains recycled polypropylene (PP) plastic waste. Perform Eng Nat Sci. https://doi.org/10.21533/pen
8. Jain A, Siddique S, Gupta T, Sharma RK, Chaudhary S (2020) Utilization of shredded waste plastic bags to improve impact and abrasion resistance of concrete. Environ Dev Sustain 22:337–362. https://doi.org/10.1007/s10668-018-0204-1
9. Wu H, Liu C, Shi S, Chen K (2020) Experimental research on the physical and mechanical properties of concrete with recycled plastic aggregates. J Renewable Mats 8:727–738. https://doi.org/10.32604/jrm.2020.09589
10. Gu L, Ozbakkaloglu T (2016) Use of recycled plastics in concrete: a critical review. Waste Man 51:19–42. https://doi.org/10.1016/j.wasman.2016.03.005
11. Raju S, Amarnath M, Anandhakumar M, Elavarasan K, Naveenkumar A (2019) Utilisation of waste plastics as a replacement of cement in paver blocks. Int Res J Eng Tech 6(3):2497–2951
12. Admile PR, Nemade PD (2020) Performance of structural concrete using recycled plastics as coarse aggregate. In: Prashant A, Sachan A, Desai C (eds) Adv comp methods and geomechanics. Springer, Singapore
13. Alenogines L, Bautista R, Sofia CN (2019) Shredded polyvinyl chloride (PVC) as substitute for the coarse aggregate in paver production. J Eng Man App Sci Tech. https://doi.org/10.14456/ITJEMAST.2019.245
14. Thorneycroft J, Orr J, Savoikar P, Ball RJ (2018) Performance of structural concrete with recycled plastic waste as a partial replacement for sand. Con Build Mats 161:63–69. https://doi.org/10.1016/j.conbuildmat.2017.11.127
15. Jacob-Vaillancourt C, Sorelli L (2018) Characterization of concrete composites with recycled plastic aggregates from post-consumer material streams. Con Build Mats 182:561–572. https://doi.org/10.1016/j.conbuildmat.2018.06.083
16. Ge Z, Sun R, Zhang K, Gao Z, Li P (2013) Physical and mechanical properties of mortar using waste Polyethylene Terephthalate bottles. Con Build Mats 44:81–86. https://doi.org/10.1016/j.conbuildmat.2013.02.073
17. Patil GN, Al Yahmedi M, Walke SM, Rao LN (2020) Manufacturing of plastic sand bricks from polypropylene and polyethylene waste plastic. Int J Adv Sci Tech 29(8):206–2068
18. Shiri ND, Kajava PV, Ranjan HV, Pais NL, Naik VM (2015) Processing of waste plastics into building materials using a plastic extruder and compression testing of plastic bricks. J Mech Eng Auto. https://doi.org/10.5923/c.jmea.201502.08
19. British Standards Institution (2002). Drainage channels for vehicular and pedestrian areas—Classification, design and testing requirements, marking and evaluation of conformity, BS EN 1433:2002. Incorporating amendment no. 1 and corrigendum no. 1
20. British Standards Institution (2003). Eurocode 1. Actions on structures. Traffic loads on bridges, BS EN 1991–2:2003
21. Design Manual for Roads and Bridges (2006). Pavement design, Vol 7 Pavement design and maintenance, Pavement design and construction. Part 3, HD 26/06
22. Highways England, manual of contract documents for highway works, Vol 1 Specification for highway works. Series 500. Clause 516 (Combined drainage systems)
23. British Standards Institution (2015). Testing concrete. Methods for analysis of hardened concrete. BS 1881–124: 2015
24. British Standards Institution (2019). BS EN 12390-3:2019. Testing hardened concrete. Compressive strength of test specimens
25. Gere JM, Timoshenko SP (1991), Mechanics of materials (3rd Ed.), Nelson Thornes Ltd., ISBN: 0–412–36880–3
26. British Standards Institution (2016). Concrete—specification, performance, production and conformity, BS EN 206:2013+A1:2016
27. British Standards Institution (2014). Eurocode 2: Design of concrete structures—Part 1–1: General rules and rules for buildings, BS EN 1992–1–1:2004+A1:2014
28. Design Manual for Roads and Bridges (2006). Traffic Assessment, Vol. 7 Pavement Design and Maintenance, Pavement Design and Construction. Part 1, HD 24/06